Results in Materials 21 (2024) 100543

Contents lists available at ScienceDirect

Results in Materials

journal homepage: www.sciencedirect.com/journal/results-in-materials

Mechanical testing of threaded inserts for additively manufactured sandwich panels with Gyroid core structures

David Lohuis [a,*,1], Hendrik Traub [a,1], Christian Hühne [a,b]

[a] Technische Universität Braunschweig, Institute of Mechanics and Adaptronics, Langer Kamp 6, 38106, Braunschweig, Germany
[b] German Aerospace Center, Institute of Composite Structures and Adaptive Systems, Lilienthalplatz 7, 38108, Braunschweig, Germany

ARTICLE INFO

Keywords:
Threaded insert
TPMS
Sandwich
Honeycomb
SLA
Moment of area

ABSTRACT

Additively manufactured sheet networks with low relative density show significant load-bearing capabilities while fulfilling additional requirements such as conducting gases. Introducing sheet networks as a core structure in sandwich panels requires fastening points for panel installation. This study develops, manufactures and mechanically investigates fastening points for triply periodic minimal surface sheet networks. While two concepts for Gyroid sheet networks are derived from an existing Honeycomb concept, a third concept improves the load-to-weight ratio by functionally grading the Gyroid's relative density. Pull-out tests were conducted to compare the performance of the insert concepts integrated into the Honeycomb and Gyroid sandwich specimens. The tests showed that only the functionally graded Gyroid concept reaches a significantly higher load-to-weight ratio than the Honeycomb concept, suggesting that its modified structure is effective. A numerical comparison of the Honeycomb's and Gyroid's unit cells shows equal moments of area for equal relative densities, thereby underlining the same load-bearing capabilities for similar insert concepts. In contrast to the Honeycomb fastening points, the Gyroid fastening points show a significant load-bearing capacity after the initial failure, which results in a residual load-bearing capability and, therefore, increased system robustness.

1. Introduction

Sandwich panels are commonly used in aerospace engineering due to their high stiffness-to-weight ratio. While core materials such as polymeric foams, metal foams, and balsa wood are well established in general engineering [1], in the aerospace industry, aluminium Honeycombs are widely spread [2]. Additive manufacturing processes offer the possibility of producing core structures with good mechanical characteristics at low relative densities (*RD*), such as lattice structures and triply periodic minimal surfaces (TPMS) [3,4]. New core structures have the potential for additional weight savings and functional integration into the sandwich panel core structure. One recent example for functional integration of sandwich panels are additively manufactured suction panels for the laminarisation of transport aircraft [5].

To use the high stiffness-to-weight ratio of sandwich panels, fastening points for local load introduction with equally high mechanical properties are needed. While many types of threaded inserts exist for traditional Honeycomb-core sandwich structures [6] and lattice structures [7–9], no fastening solutions are available for TPMS-core sandwich panels. Most available research on TPMS focuses on understanding their mechanical behaviour [4,10].

This paper aims to develop a local load introduction concept for TPMS-core sandwich panels, focusing on suction panels for hybrid laminar flow control introduced in Ref. [5]. Existing solutions for Honeycomb sandwich panels and insight into the load distribution of TPMS sandwich panels are used as a starting point for this development. This study focuses on different insert concepts and uses Gyroid sheet networks to represent TPMS sheet networks. All TPMS sheet networks, including Gyroid, share the open-cell architecture, a three-dimensional spatial extension, and similar mechanical properties [4].

First impressions of load distribution in TPMS sandwich panels are provided by Fashanu et al. [11] and Alshaer et al. [12], which experimentally compared them to Honeycomb sandwich panels in three-point bending tests. These authors apply a line load across the entire width in the middle of the face sheet, and although it differs from a punctual load caused by a threaded insert, the authors of this study assume a comparable load distribution inside the panel. A review of both papers revealed some inconsistencies between their results. While Fashanu et al. claim

* Corresponding author.
E-mail addresses: david.lohuis@tu-braunschweig.de (D. Lohuis), h.traub@tu-braunschweig.de (H. Traub), christian.huehne@dlr.de (C. Hühne).
[1] These authors contributed equally to this work.

https://doi.org/10.1016/j.rinma.2024.100543
Received 13 September 2023; Received in revised form 17 January 2024; Accepted 5 February 2024
Available online 13 February 2024

that a Honeycomb core has a higher pull-put load and stiffness than a Gyroid core, Alshaer et al. suggest the opposite. Their data indicate that the Gyroid core has almost twice the specific stiffness and more than twice the specific pull-out load of the Honeycomb reference. Therefore, it is an additional objective in this study to generate more data to provide further insight into the inconsistencies of both studies.

Different approaches exist to further increase the load-to-weight ratio of threaded inserts. One of them is to optimize the core structure in the vicinity of the insert, i.e. by topology optimization. For a Honeycomb core, this approach has been explored by Schwenke and Kruse [13] and Schulte et al. [14], where they discovered an average increase in pull-out load of about 120% and average increase in stiffness of about 50%, due to the topology optimization. They started with a solid cylinder around the insert and reduced its density in multiple FEM iterations. Their result was a star-shaped structure where the arms fade with increasing radius. The star structure is superposed with the core and finally additively manufactured.

This study implements a different approach, where a relative density gradient of the core structure in the vicinity of the insert is expected to reduce the load-to-mass ratio. The topology optimization approach and functional grading both adapt the mass around the insert to fit the stress state in the material. The main advantage of functional grading is that its effectiveness can be described with a simple analytical approach. It does not require sophisticated numerical approaches and calculations. Functional grading is also an integral part of the existing core structure. No additional parts are introduced.

In summary, this study develops fastening points for TPMS sheet networks by integrating and testing traditional threaded inserts for Honeycombs at the example of Gyroid sheet networks. This paper presents three concepts for integrating threaded inserts into Gyroid sheet networks. The first concept makes no changes in the structure except for the void where the insert is integrated. The second concept limits the distribution volume for the adhesive with an additional wall. The third and most advanced concept uses functional grading of the Gyroid structure in the vicinity of the insert for a beneficial distribution of the adhesive and advantageous load introduction into the sandwich core. Sandwich panels for all three concepts are manufactured on stereolithography printers [15] and tested with pull-out tests to characterise their mechanical behaviour. Honeycomb panels are manufactured and tested with the same procedure to benchmark the Gyroid insert concepts. A numerical comparison of the Gyroid's and Honeycomb's moment of area allows to include the mechanical characteristics of the panel itself in the discussion of the experimental results.

2. Development of fastening point concepts

In contrast to Honeycombs, TPMS form a porous, fully curved structure only manufacturable with additive technology. One advantage of additive manufacturing of sandwich panels is the possibility for significant function integration and the local variation of the panel geometry. This allows designing the structure in the vicinity of fastening points to integrate threaded inserts. While in Honeycomb sandwich panels the voids for the insert integration are usually cut into the core structure after the manufacturing of the panel, additive manufacturing allows the integration of the voids during manufacturing. Functional grading of the Gyroid structure in the vicinity of the insert allows controlling how far the adhesive reaches into the structure and, therefore, directly affects the mechanical characteristics of the fastening point.

The fastening concepts for TPMS developed in this paper are designed to attach suction panels for hybrid laminar flow control. To avoid interference with the high-quality suction surface, the insert can only be integrated from one side of the sandwich panel. Additionally, air must be able to flow through the sandwich core. Not the entire height of the core can, therefore, be used for the insert. The partially potted insert concept which can be found for Honeycomb sandwich panels [6,16,17] meets both conditions and is chosen in this study as a template for further developments. Fig. 1 shows the image and conceptional sketch of a partially potted insert in a Honeycomb core.

For the integration of partially potted inserts into Honeycomb cores, the structure is cut and an insert is placed inside the hole. The insert, shown in grey in Fig. 1, is a threaded metal rod with two flanges, one at the bottom and one at the top. In the top one are two holes. An adhesive can be inserted through one hole to fill the cavity and establish a physical connection, the so-called potting, between the core and the insert. The other hole ensures venting of the residual air in the cavity and, therefore, its complete filling with adhesive compound.

Loads must pass through two distinct interfaces when a pulling force is applied to the insert. The first interface is the boundary between the polymer adhesive and the threaded insert. This interface is the same for Honeycomb and Gyroid concepts and discussed by Cushman [16]. This study, in contrast, focuses on the second boundary, between the polymer adhesive and sandwich core, where forces are distributed into the core and face sheet. While shear forces transfer the load into the Honeycomb core, compression forces transfer the load into the face sheet. Several studies [16–18] show that the polymer and core load transfer is the weaker interface and, therefore, of higher interest. The surface area between the core and polymer adhesive is called the bonding area A_{bond}, and in combination with the mechanical characteristics of the bonding, it dictates how much load can be introduced to the sandwich core. Increasing the potting diameter or height increases the bonding area and, therefore, allows the application of higher pulling forces at the insert.

Adapting the partially potted Honeycomb concept for a Gyroid sheet network without modifications leads to a straightforward approach, shown by the unrestricted concept of Fig. 2. While the porosity of TPMS is advantageous for suction panels, it allows the adhesive to distribute far into the TPMS structure, preventing the bonding of the insert and core structure. An adhesive with linear viscosity is expected to move away from the insert, resulting in a poor or no connection to the core. High connectivity between the insert and the core is far more likely when using an adhesive with thixotropic flow characteristics. Thixotropic adhesives have a non-linear flow behaviour where they are less

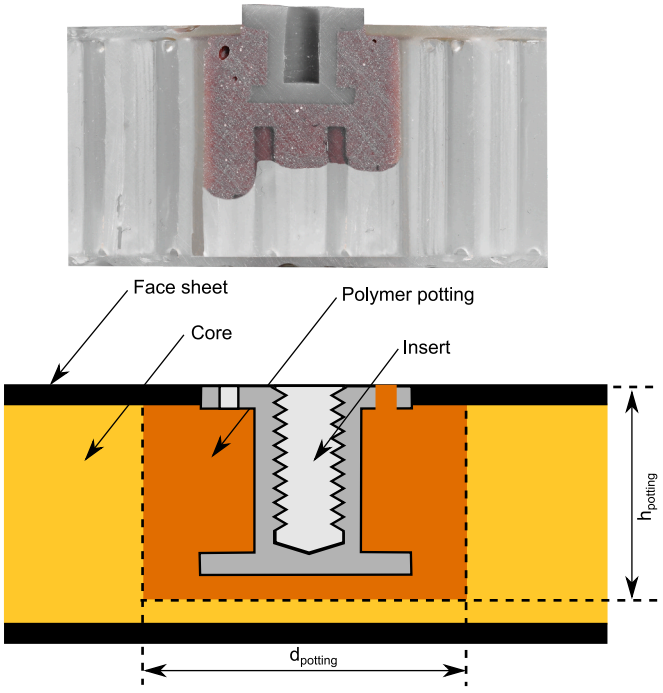

Fig. 1. Visualisation of the partially potted insert concept in a printed Honeycomb core (upper). Schematic diagram of a partially potted insert concept with important design parameters (lower).

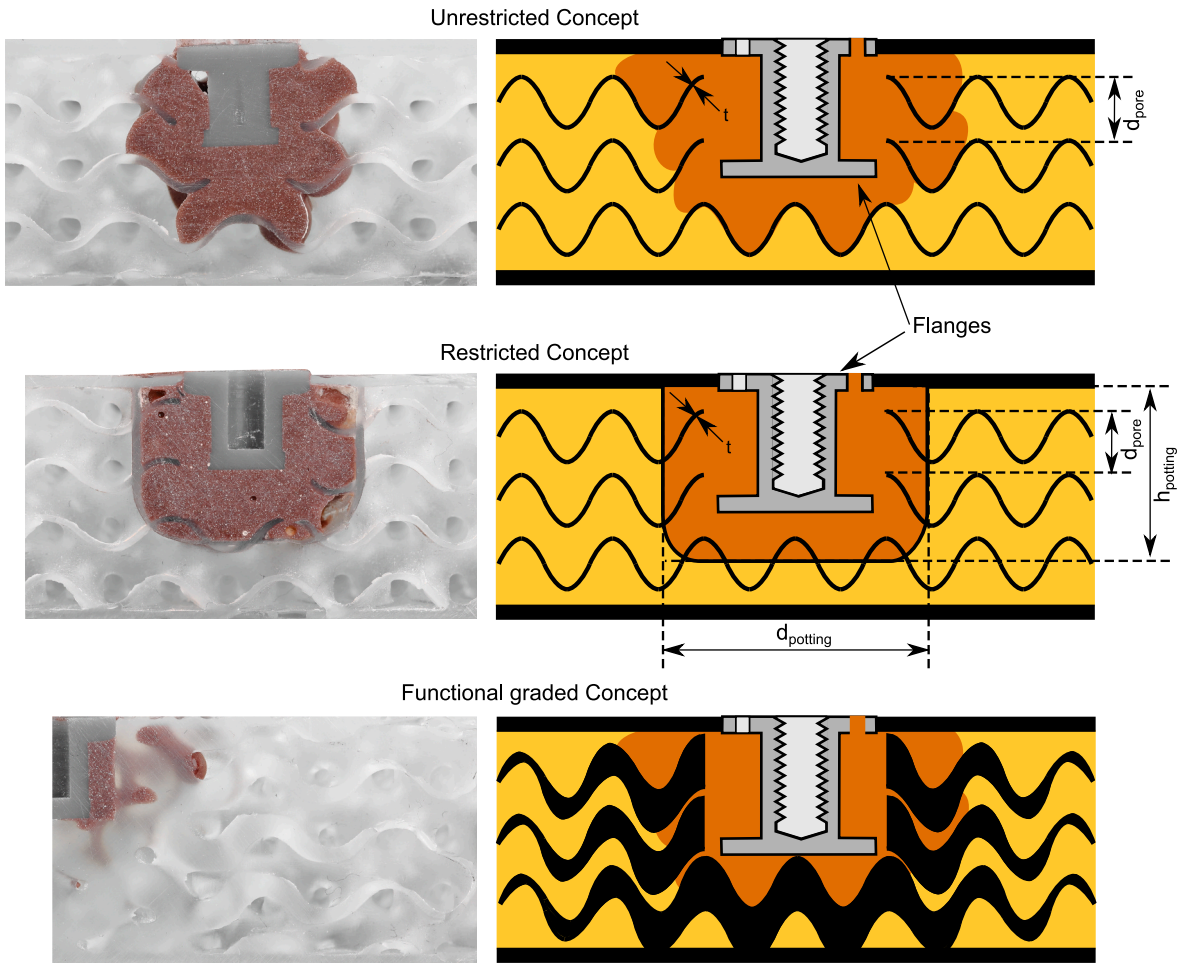

Fig. 2. Photographs of all three load introduction concepts in a Gyroid structure (left). Schematic of the concepts, including the main important design parameters (right).

viscous in a flowing than in a static state. The assembly of plastic dummy inserts into a Gyroid structure with the thixotropic adhesive Scotch-Weld 9300 B/A FST [19] revealed decent results, where the adhesive does not leave the sandwich boundaries or accumulates at the bottom.

A restricted concept is proposed for polymer adhesives with low viscosity and no thixotropic properties, where a physical boundary inside the core prevents the adhesive from spreading into the sandwich. The restriction is an artificial wall which surrounds the insert and limits the spreading. Such a wall can be directly integrated into the Gyroid core structure, as demonstrated in Fig. 2.

Both concepts have different advantages and disadvantages. The unrestricted concept is less susceptible to cavities inside the polymer potting since air can vent through the Gyroid core structure. A hole for venting at the top is thereby not required. On the other hand, potting diameter and height are not precisely defined and vary between individual specimens. Hence, a higher variance in the maximum pull-out force is expected. The restricted concept has inversed advantages and disadvantages compared to the unrestricted. It is highly susceptible to cavities but has a well-defined potting geometry. Both concepts are further investigated in this study because details of their mechanical behaviour are unclear, and they have their advantages.

In the restricted and unrestricted concept, the Gyroid structure overlaps with the potting, creating a macroscopic form fit of the potting and the core structure. Therefore, in addition to the existing potting diameter and height, two new design parameters are added, the pore size and wall thickness. Both are determined by the relative density and surface-to-volume ratio A/V of the TPMS structure. When the polymer flows into the channels of the Gyroid structure, it develops a Gyroid solid network, which is the inverse of the Gyroid sheet network. In this case, the solid network only fills a small region around the insert. The region is not large enough so that it repeats itself and thus creates a formation comparable to branches. The amount of branches rises with increasing potting diameter, decreasing the loading in each branch. How much load a specific branch can carry depends on its thickness and length. Load is continuously transferred to the Gyroid structure over the length of the branch. After a certain distance, the entire load is transferred to the Gyroid wall. The quotient of wall thickness and branch diameter and the according strength determines when and where the structure fails. The best-case scenario is reached when the interfacing Gyroid solid and sheet network parameters are designed so that both structures fail simultaneously.

Functional grading of the Gyroid sheet network in the proximity of the threaded insert is created by modifying the relative density as indicated in Fig. 2. It has the potential to significantly increase the efficiency of the load introduction, which is defined as the ratio between the maximum load and the mass of the insert and potting. This ratio is often not optimal in traditional inserts and worsens when introducing higher loads to the structure. This is illustrated with a simple model expressed by equations (1) and (2). Both depend on the insert radius, where the mass is proportional to the radius squared while the force is proportional to the potting surface and consequently has a linear relationship. Therefore, the efficiency drops with increasing insert diameter. To reach maximum efficiency for all insert sizes, the relation given by equation (3) must become independent of the insert geometry. The

relative density influences the shear strength and the density in the equation. Functional grading can, therefore, be used to manipulate the efficiency of the insert and increase it to its maximum in an optimal case.

$$F_{max} = 2\pi r h \tau_{max} \tag{1}$$

$$m_{pot} = \pi r^2 h \rho \tag{2}$$

$$\frac{F_{max}}{m_{pot}} = \frac{2\tau_{max}}{r\rho} \tag{3}$$

According to the model of Thomson [20], the shear stress near the threaded insert decreases hyperbolically with increasing radius, which means that the shear strength must follow the same trend to be as efficient as possible. A qualitative example of the stress and strength curve is given in Fig. 3. While the stress is displayed as a solid blue line, the strength is displayed as a dashed orange line. In the unrestricted concept, the strength jumps at every material interface due to stiffness changes. The blue line must stay below the orange line to prevent the structure from failing. The hatched area between both curves illustrates the unused strength potential of the structure, causing unloaded mass. Minimizing the hatched area is equal to maximizing the force-to-mass ratio and, thus, the efficiency. A hyperbolic relative strength trend achieves a minimal area, as shown in the sub-figure of the graded concept.

In Fig. 3, the internal stress curve contains two stress peaks, which are potential points of failure and must be reduced to a minimum. The peaks arise from Thomson's [20] model for internal stress and appear wherever the stiffness shows discontinuities, for example, at material boundaries. The difference in stiffness is proportional to the height of the peak. The results of Bozhevolnaya et al. [21] indicate that the stress peaks can be reduced by inserting a ring with a different material between the threaded insert and the polymer potting. The ring exhibits an intermediate stiffness compared to the surrounding materials, resulting in additional but lower stress peaks. Increasing the number of boundaries up to infinity would lead to the ideal situation, where all stress peaks would disappear completely due to a completely smooth stiffness transition. Cellular solids allow a continuous stiffness transition by manipulating their relative density. Therefore, functional grading not only allows the stress and strength curve to have a similar shape but also reduces the stress peaks, bringing the two curves closer together and maximizing the pull-out load of the threaded insert further.

3. Specimen design and experimental setup

This study experimentally investigates threaded inserts for TPMS sheet networks regarding their stiffness and pull-out load characteristics in pull-out tests. For this purpose, TPMS sandwich panels are additively manufactured, integrating three different concepts for threaded inserts. While the TPMS sandwich panels can be manufactured as a single integral part, Honeycomb sandwich panels manufactured for comparison need to be assembled from a printed core and printed face sheets. Integral manufacturing of Honeycomb panels is impossible on stereolithography (SLA) printers as liquid resin residues would become trapped inside the closed panel. All insert concepts are then tested with a pull-out test in a custom-made test setup, initially developed by Wolff et al. [22] for their Honeycomb inserts.

This study uses a set of five test specimens for each of the three TPMS concepts and for the Honeycomb concept to statistically determine the pull-out load and performance of the threaded inserts. The results can be directly compared when all specimens share the same geometry. Both face sheets are 1 mm thick over an area of 120 mm × 120 mm. The core between the face sheets is $h_c = 20$ mm high so the whole structure has a

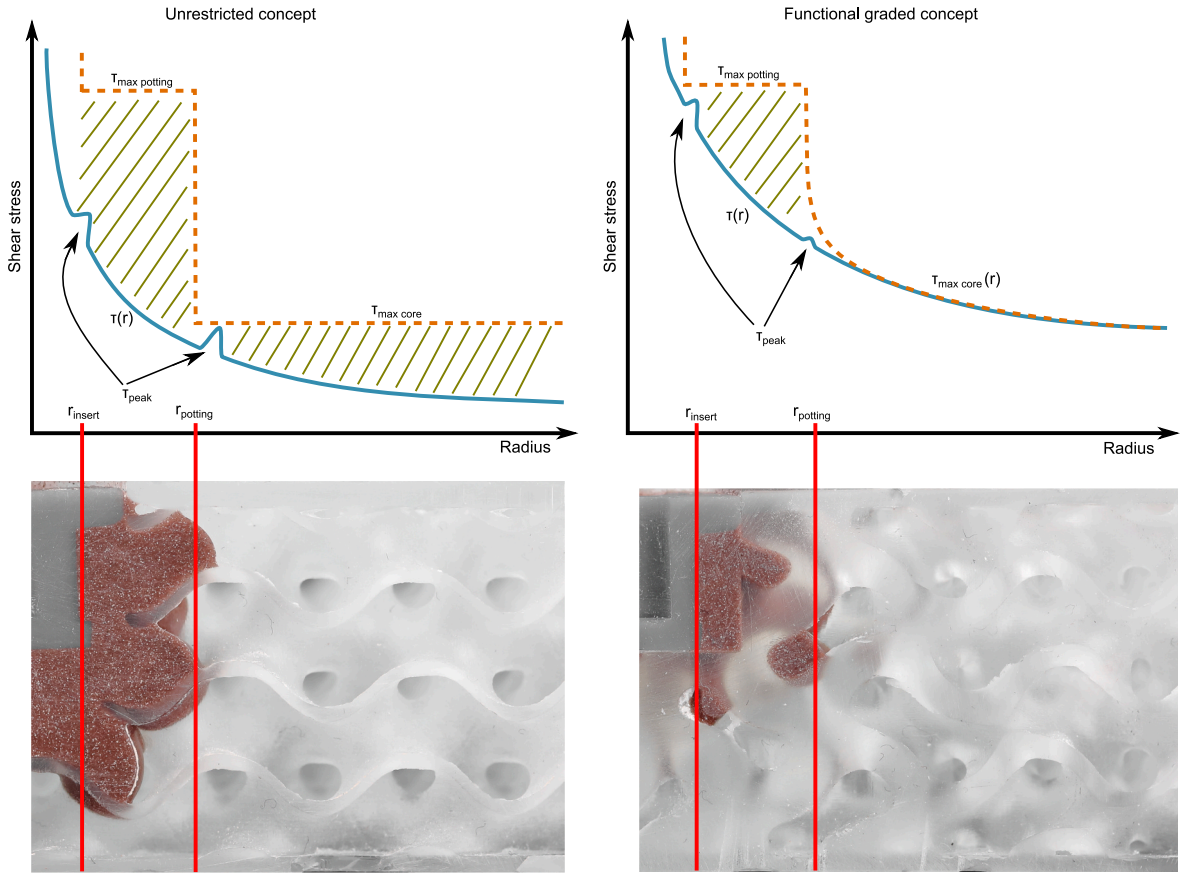

Fig. 3. Shear stress and strength curve for a sandwich structure with and without functional grading. The hatched area is a metric for the mass optimization potential. A smaller area means a more efficient load introduction.

height of 22 mm. Comparable core structures are established by choosing the same relative density. It is assumed that the same relative density of the core leads to equivalent moments of area and, therefore, to equivalent mechanical properties. Table 1 shows the global geometrical data for all specimen types.

A suitable Insert for the given sandwich size is the NAS1836-08-11 [23]. It is also available in large quantities and commonly used in the aerospace industry. The insert diameter at the top is $d_I = 11.4$ mm and the height is $h_I = 8.9$ mm.

3.1. Specimen design

Specific dimensions for the potting inside the Honeycomb specimens must be established to be translated to the Gyroid concepts. The insert design handbook [24] published by the European Corporation for Space Standardization (ECSS) contains state-of-the-art rules for Honeycomb potting dimensions and is therefore used to derive the dimensions. The design rules provide relationships which are used to determine the potting dimensions dependent on the Honeycomb cell size. It also provides a simplified model to calculate the pull-out load of an insert for a given potting and core geometry. Potting diameter and height are calculated according to equations (4) and (5) as given by the handbook. They are employed to obtain the potting height and diameter values as specified in Table 2.

$$d_p = d_I + 0.8 * l_{uc} \tag{4}$$

$$h_p = h_I + 7 \tag{5}$$

The ECSS insert design handbook only refers to Honeycomb structures manufactured from thin aluminium foil. In this work, the Honeycomb core must be made of the same material as the Gyroid core to maintain comparability. Used in this study for manufacturing the specimen, the Formlabs Form 3 L SLA printer [15] achieves a minimum wall thickness of about $t = 0.3$ mm. A wall thickness of $t = 0.5$ mm ensures a uniform wall thickness across the Gyroid structure and is therefore used for the two cores. According to the ECSS insert design handbook, the most common cell sizes for aluminium foil Honeycombs are 3.2 mm or 4.8 mm and reach relative densities of 1.6% and 1% respectively. Large cell sizes are required to achieve similar relative densities with additively manufactured Honeycombs compared to the insert size. Large cells, however, are out of the scope of the design rules and lead to an oversized potting diameter. While thick-walled printed Honeycombs increase their shear strength compared to thin-walled aluminium Honeycombs, the thermoset material decreases their shear strength. With a one to two orders of magnitude lower thermoset shear strength than aluminium shear strength, the opposing effects of wall thickness and material strength partially compensate each other. Whether the design rules defined by the ECSS insert design handbook are valid for thick-walled thermoset Honeycombs remains to be validated. However it is assumed for this study so that thick-walled Honeycombs with regular cell sizes and higher relative densities are used for further experiments.

The authors derive an analytical formula for the relative density of Honeycombs in Appendix B, given in equation (6), and an approximation for the relative density of Gyroids as described by equation (7) derived from Ref. [4] with an additional cubic factor for high relative densities. For Honeycomb and Gyroid structures, the non-linear term can be neglected for small relative densities below $RD < 0.3$. In both relationships, the relative density depends on the unit cell length l_{uc} and wall thickness t.

$$RD_H = 2 * \frac{t}{l_{uc}} - \frac{t^2}{l_{uc}^2} \tag{6}$$

$$RD_G \approx 3.09\frac{t}{l_{uc}} - 0.04\left(\frac{t}{l_{uc}}\right)^3 \quad (R^2 = 0.999999995) \tag{7}$$

For the Honeycomb and Gyroid core structures, the relative density has been fixed to a value of 15%, while the wall thickness has been set to its minimum value of $t = 0.5$ mm. This set of parameters results in a cell size where more than one complete Gyroid cell fits inside the core height and is therefore appropriate for the given sandwich height. At this relative density and wall thickness, the honeycomb cells have a size of $l_{uc} = 6.66$ mm that ensures that multiple cells are filled with adhesive while matching the calculated potting diameter. The authors assume the chosen parameters result in mechanically equal sandwich structures and establish comparability between them.

While the ESA handbook provides guidelines for dimensioning potting and threaded inserts for Honeycomb sandwich structures, no such guidelines are available for TPMS sandwich structures. Developing an analytical design rule for the dimensioning of threaded inserts for TPMS sandwich panels seems unrealistic due to the three-dimensional character of the TPMS sheet networks. Therefore, the authors of this study decided to use the design guidelines for Honeycomb structures to dimension the inserts for TPMS sheet networks.

A big difference between a Honeycomb and a Gyroid cell is that the pores are a three-dimensional continuous channel network in a Gyroid cell. The network continuity allows arbitrary potting dimensions, while Honeycombs must have discrete and irregular potting dimensions. While the number and size of honeycomb cells filled with potting determine the potting dimensions, cell size and potting diameter of Gyroid inserts can be designed independently.

A thin wall limits the potting radius and height in the restricted concept. Since the ESA handbook defines the potting radius and height, these parameters can be used to design the wall integrated into the Gyroid structure, shown in Fig. 2. For a wall thickness of $t = 0.5$ mm and 15 % relative density, equation (7) yields a cell size of $l_{uc} = 10.31$ mm. The wall which contains the potting is only 0.3 mm thick because it is not supposed to carry any load. A 5 mm radius is added at the bottom to decrease the probability of cavities in the corner. Between the insert and the core structure is a 1 mm gap, which allows the polymer to flow underneath the insert.

To create an equivalent potting in the unrestricted concept, the polymer, which is filled into the structure, is assumed to spread evenly in all directions. Introducing the same polymer volume as in the other concepts leads to comparable geometries. The polymer volume for the potting is calculated according to equation (8). The polymer volume for the unrestricted concept is calculated from the design rules for honeycombs, the volume of the metal insert and the relative density as illustrated by equation (8). Since it is the same as the polymer volume of the restricted concept, it can also be extracted from the CAD model. Both ways lead to a polymer volume of about 2424.56 mm^3, which is equal to about 2.4 mL.

Table 1
Overview of the specimens' general dimensions.

Parameter:	h_c	h_f	RD	l_{uc}	t
Unit:	[mm]	[mm]	[%]	[mm]	[mm]
Honey	20.0	1.0	15	6.66	0.5
G-RE	20.0	1.0	15	10.47	0.5
G-UR	20.0	1.0	15	10.47	0.5
G-FG	20.0	1.0	70–15	10.47	2.33–0.5

Table 2
Overview of the specimens' potting dimenstions.

Parameter:	d_I	h_I	d_p	h_p	V_p
Unit:	[mm]	[mm]	[mm]	[mm]	[ml]
Honey	11.4	8.9	16.7	15.9	n.a.
G-RE	11.4	8.9	16.7	15.9	2.4
G-UR	11.4	8.9	n.a.	n.a.	2.4
G-FG	11.4	8.9	n.a.	n.a	1

$$V_{Polymer} = (1 - RD) * (V_{Pot.} - V_{Insert}) \quad (8)$$

The functionally graded concept has more parameters which need to be determined. Close to the insert, the relative density is set to 70%. A higher value would further reduce the stiffness jump between the potting and core and weaken the polymer potting due to small branch diameters. The relative density remains constant within a radius of 8.35 mm. Filling this area with polymer would lead to a cylinder which is completely filled with material, while its size is comparable to the cylinder of the restricted and unrestricted concept. A constant relative density of the Gyroid structure within this area simplifies the calculation of the amount of polymer. It has been determined with equation (8) to a value of 855.73 mm^3 and rounded to 1 mL for manufacturing purposes.

The relative density grading is defined by a function returning the relative density depending on the radius from the insert centre line. Between a radius of 8.35 mm and 30 mm, the relative density decreases linearly, as shown in the upper part of Fig. 4. Cubic splines at both ends establish a smooth transition to the constant regions. This type of functional grading is only a first approximation. An optimized gradient could not be computed because the relationship between the relative density and the material's shear strength is needed but not known yet.

The three-dimensional shape of the relative density grading is a half-ellipsoid. A spherical shape is preferred over a cylindrical one because the inserts are developed for a laminar flow control system and with a cylindrical gradient a fluid flow at the lower face sheet is less affected. In this configuration, the short radius of the ellipsoid fits the sandwich core height, while the long radius is set to 30 mm. The ellipsoid can be calculated as a distorted sphere with equation (9), where the factor k distorts the sphere according to the sandwich height. Inside the region of the half-ellipsoid, the density decreases from 70% at the inside to 15% at the outer radius. Fig. 4 illustrates the complete geometry and gradient parameters.

$$r = \sqrt{x^2 + y^2 + k * z^2} \quad (9)$$

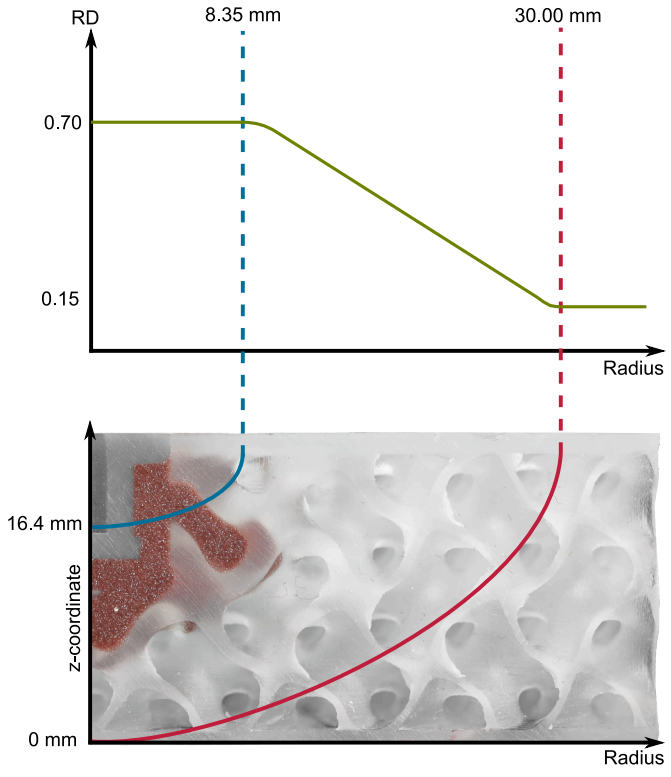

Fig. 4. Relative density trend dependent on the radius (upper). Positions of the relative density gradient boundaries (lower).

$$k = \left(\frac{R_{max}}{z_{max}}\right)^2 \quad (10)$$

Four different specimen sets were created to investigate the local load introduction in sandwich plates with Gyroid cores. A standardized nomenclature system has been established for characterizing various types of specimens, wherein honeycomb structures are denoted by the letter "H ", while Gyroid specimens with walls and without walls are abbreviated as "G-RE" and "G-UR". Gyroid specimens possessing a gradient are denoted by the acronym "G-FG". Each of the four sets contains five specimens of one specimen type.

3.2. Manufacturing techniques of the different specimens

Additive manufacturing is always controlled by a computer and, therefore, needs digital information about the part's geometry. Usually, part geometry is created through CAD software. Fusion 360 [25] has been used to design the Honeycomb sandwich plates, while complex TPMS cells with 3D surfaces can not be created with state-of-the-art CAD software. A simple and fast way is provided by the Python SDF library [26], where geometry is described by implicit equations instead of surfaces. It uses the marching cubes algorithm to convert the geometry into a triangle mesh. The resulting mesh is saved in STL file format, which can be further processed by a slicing software.

All panels in this study are printed on a Formlabs Form 3 L SLA printer in Clear v4 [27] resin with a layer height of 50 µm. Residual resin is removed in a Form Wash L [28] isopropanol washing machine for 10 min, following the material data sheet [29]. To reach the full mechanical properties of the material, the clean parts are post-cured in the Form Cure L UV light oven for 30 min at 60 °C.

Due to their closed-cell structure, the Honeycomb sandwich panels can not be manufactured as an integral part. It prevents uncured resin from exiting the cells. With one face sheet being printed separately, the resin can be removed from all cavities after printing. In an extra manufacturing step, the face sheets are bonded to the Honeycomb core using 5 min Epoxy by the company Toolcraft. Preliminary tests showed that 4 g–5 g of epoxy loaded with a weight of 35 kg are required to form a visually proper bond. While less adhesive did not coat the entire surface, less weight was not enough to flatten the surface to establish contact over the whole area. The insert was glued into the completed sandwich by using the specialized adhesive "Scotch-Weld 9300 B/A FST" from 3 M [19]. Before the insert is put into place and filled with adhesive, a small amount of the adhesive is filled into the cavities of the honeycomb cells so that air is trapped at the bottom of the cells. The air ensures that no mechanical contact is established between the potting and the bottom face sheet when the rest of the adhesive is inserted. Mechanical contact between the insert and bottom face sheet must be avoided since it would lead to a fully potted insert concept and, therefore, would destroy all comparability to the other concepts.

As part of the manufacturing process, the quality has been inspected by measuring the main important dimensions and weight. Measurements uncovered that 4 out of 6 walls of each Honeycomb unit cell are twice as thick as planned. Consequently the relative density of the core is also higher than expected and therefore also higher compared to the Gyroid specimen sets. The exact differences are documented in Table 3.

Manufacturing the different types of Gyroid sandwiches did not

Table 3
Relative Core Density extracted from the STL files and measured data. Measured data is averaged over the whole specimen set. A material density of 1.145 kg/mm^3 has been used to calculate the relative density via the measured mass.

	Honey	G-RE	G-UR	G-FG
Model	14.5%	14.7%	14.6%	16.6%
Measured	24.0%	20.2%	17.8%	19.8%
Difference	9.5p.p.	5.5p.p	3.2p.p	3.2p.p

result in any issues. Relative densities deviated only a few per cent from the anticipated value as documented in 3. Such deviations are nominal compared to additively manufactured sandwiches in other studies [11]. Specimen from the set G-RE have been filled with polymer prior to the insert integration. This sequence allows air to exhaust from sharp corners before adding the insert. In contrast, the specimen set G-UR allows adding polymers only through the insert because the open-cell core architecture allows air to exit through the core. Assembling inserts in the G-UR specimens took about half the time because no air was removed by hand.

The final potting masses of all specimens are summarised in Table A.8 in Appendix A. It also includes statistical metrics like the average, variance and standard deviation. A comparison between the variances of the not-optimized concepts shows that the highest variance occurs in the specimen set G-UR, which was expected due to an irregular potting diameter and height. Since no polymer is inserted into the sandwich in advance, this concept offers the highest potential to be automated in the future, possibly leading to a lower variance in the mechanical data as well.

3.3. Composition of the testing environment

The conduction of pull-out tests on threaded inserts embedded in sandwich panels requires extending the mounting apparatus of the universal testing machine. Therefore, a metal frame designed in Ref. [22] is used, which is specifically designed for pull-out tests of sandwich panels.

Introducing the necessary forces and measuring the resulting displacements during the entire pull out test is done by a rigid metal frame. Fig. 5 schematically shows the metal frame integrated into the universal testing machine “Zwick 1476” provided by the company Zwick and Roell [30]. A metal plate with a 100 mm centre hole allows placing the sandwich specimens on top of the plate while accessing the threaded insert from below, thus realising a floating bearing arrangement of the specimen. A shackle structure connects the insert to the traverse, with a metric-to-imperial adapter at the top of the shackle. While the displacement of the screw is measured directly at the adapter with an inductive displacement sensor, the force is measured with a 100 kN load cell mounted between the shackle and the traverse. At both ends of the complete system, a cardan joint is placed to ensure that specimens are not loaded with any other forces and moments except the pull-out load.

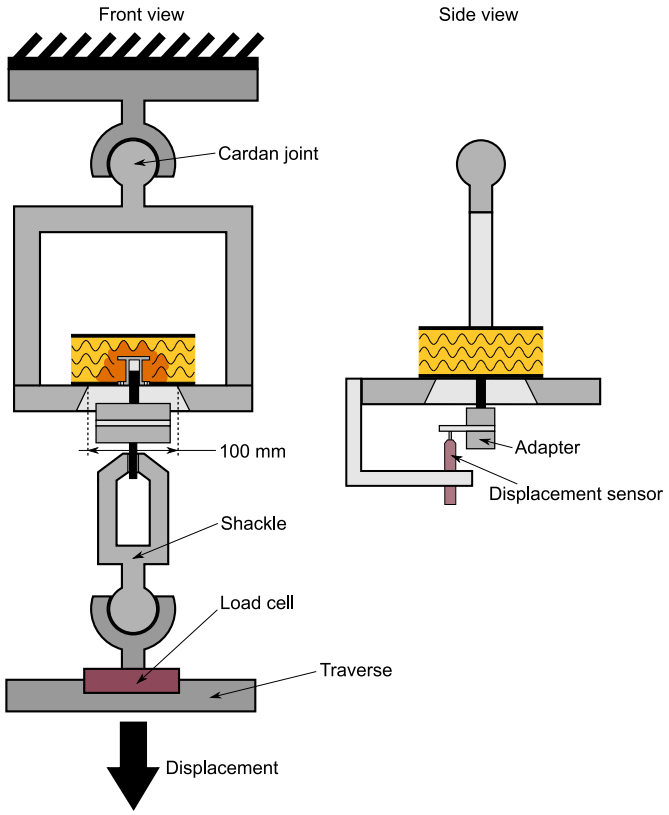

Fig. 5. Schematic front and side view of the experimental setup.

All specimens are conditioned by placing them in the laboratory 48 h prior to the first test at standardized conditions of 65 % humidity and 20 °C according to DIN EN ISO 139 [31]. After installing the testing apparatus in the test machine, all joints are straightened to minimise slipping effects. To achieve this, a solid steel plate is mounted instead of a specimen and loaded with a force of 30 kN.

The same testing procedure is applied to every specimen. First, the specimen is placed upside down at the centre of the metal frame. It is then loaded with 20 N–40 N to secure it against sideways slipping. At this point, the automated test protocol of the testing machine is turned on. It pre-loads the specimen even further up to 150 N. At this point, the traverse starts moving with a constant speed of 2 mm/min to conduct the experiment. The Experiment ends when the load drops to 50 % of its maximum value. For two of the five specimens of each set, the experiment is terminated after the first load drop so that the first failure mode can be observed.

4. Outlining the experimental results

Two types of data were produced during mechanical testing. Pictures and visual observations are used to gain insight into the fracture growth, while the data from the force and displacement sensors provides information about mechanical values like pull-out load and stiffness.

4.1. Observations about fracture growth

To identify the sequence and form of the sandwich panel failure, the authors and two camera systems observed the pull-out experiments. The dominating failure characteristic for all specimens are two major radial cracks occurring in the top face sheet as displayed in Fig. 6. In most cases, they are 180° apart and therefore split the upper face sheet into two halves, while the lower face sheet stays completely intact. Due to the symmetry of the sandwich, the compressive stress in the lower face sheet is equal to the tensile stress in the upper face sheet. The upper face sheet fails first since the tensile strength is lower than the compressive strength. This failure sequence suggests that the core structure is oversized relative to the face sheets. This core-dominated behaviour of the sandwich panel is intended in this study because it focuses on the core structure itself. In contrast, numerous other studies test sandwich panels with weaker cores that fail under shear load [6,16–18,32]

The cracks in the upper face sheet can be divided into radial and circumferential cracks. Both types originate near the potting and core interface, where the potting has the smallest radius due to the honeycomb pattern. According to Thomson’s model [20], internal forces are higher close to the insert, and stress decreases hyperbolically with increasing radius. Stress peaks arise in Thomson’s model due to a stiffness jump at the potting boundaries [21]. The origin of the cracks close to the smallest radius of the potting suggests the validity of Thomson’s model and shows that the conducted experiments are appropriate to identify the potential of different insert types.

The cracks which split the upper face sheet into two halves have different effects on Gyroid and Honeycomb cores. The Honeycomb cores show no resistance against penetration of the surface cracks. It can be observed that the cracks reach deep inside the core and, in some cases, almost touch the lower face sheet. Splitting the sandwich into two halves results in a complete loss of the integrity of its structure and the end of the experiment. In contrast, the crack cannot penetrate through the Gyroid core, resulting in a significant residual load-bearing capability.

The force-displacement curves provided in Fig. 7 underline the

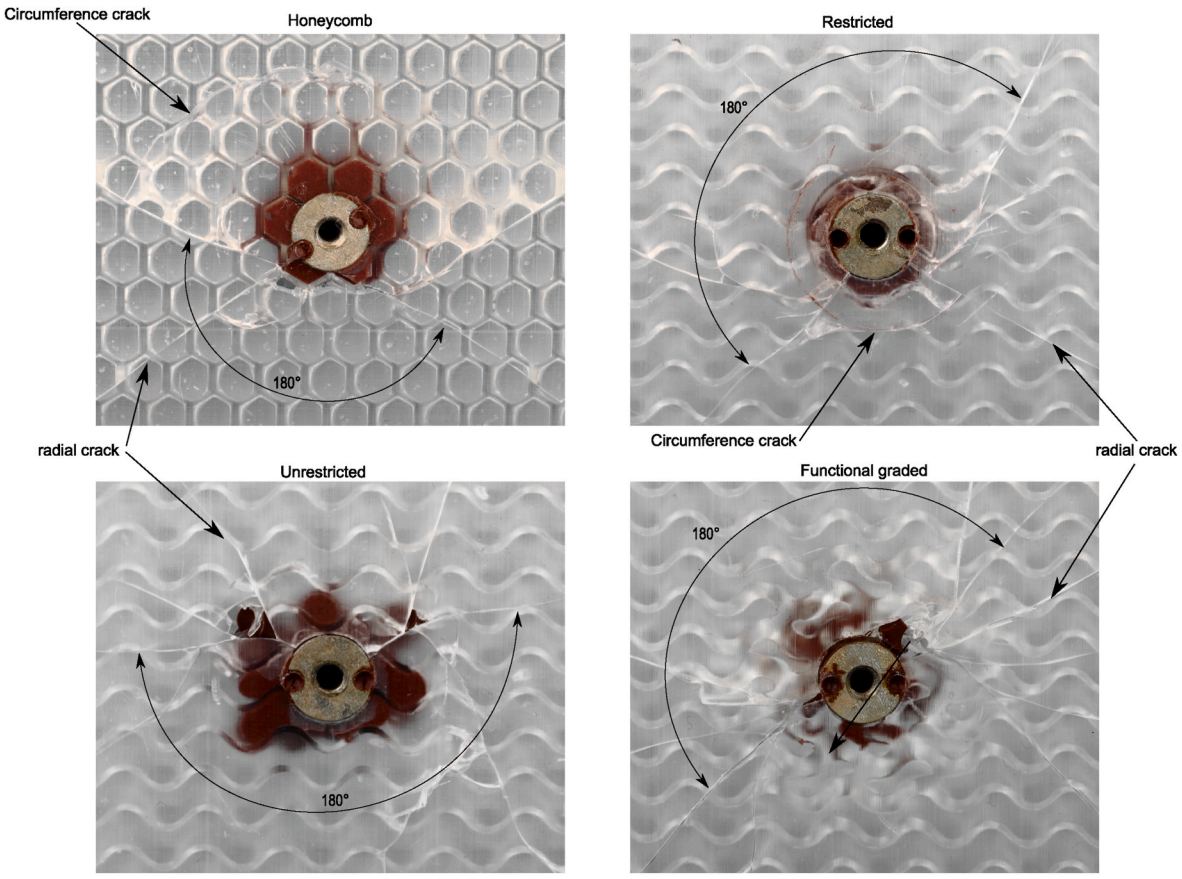

Fig. 6. Photographs of the face sheets of the specimens H5, G-RE5, G-UR2 and G-FG4.

observation that the whole integrity of the Honeycomb sandwich can be lost in spontaneous failure. The forces measured for the Honeycomb specimens constantly grow until they reach their maximum. At this point, the force drops instantly below 50 % of its maximum value, where the experiment is terminated. The single event, therefore, corresponds to the two cracks in the upper face sheet, destroying the integrity of the sandwich panel.

A special failure mode was observed in the case of H3, where the two radial cracks in the upper face sheet could not split it in half. The structure could be further loaded until a complete pull out of the insert and potting, as well as parts of the core structure and face sheet, occurred. The fragment has the shape of a cone with a maximum diameter of about 40 mm as shown in Fig. 8. The tip of the cone has an angle of 45° relative to the symmetry axis, indicating shear failure. The main difference from the other specimens is a circumferential crack propagating inside the core instead of a radial crack splitting the upper face sheet. The integrity was lost almost instantly in both cases, resulting in the force-displacement curve of Fig. 7.

While Honeycomb specimens show spontaneous insert failure, all Gyroid specimens show progressive failure. In all specimens with Gyroid cores, cracks originating in the upper face sheet could not propagate further than 2 mm into the core. The remaining core height is still able to transfer loads. This transition to a disabled sandwich structure is consistent with the force-displacement curves in Fig. 7. All specimens with a Gyroid core begin with a continuous growing graph until they reach the maximum load. At its maximum, the graph drops a few hundred newtons and then grows again. The decrease in load drop compared to the Honeycomb specimens correlates to the residual load-bearing capability of the Gyroid core structure.

After the initial failure of the Gyroid specimens, the load-displacement curve shows a distinctive saw-tooth pattern. A new crack forms whenever the force drops and a new sawtooth is completed. As long as a new tooth is created, the cracks are stopped so that there is enough Gyroid structure left to start bearing load again. The many saw teeth in Fig. 7 occurring in all three gyroid concepts indicate that multiple cracks are formed sequentially. These results demonstrate the effective crack-stopping behaviour of the Gyroid structure.

The crack-stopping behaviour of Gyroid structures leads to a completely different fracture pattern after a complete pull-out. These patterns can be observed in Fig. 8. After the upper face sheet fails, small cracks start to separate one side of the insert from the core. Only when one side of the insert is completely detached does the other side start to fail. The boundary conditions become asymmetric, and the other side shears off, including the face sheet and core material.

It is unique to the specimens with functional grading that the polymer pottings were broken after testing. The grading led to smaller polymer branches, which failed earlier than the core. It suggests a ratio between the branch diameter and wall thickness that is not properly balanced according to the strength properties of the materials. However, individual branches failing one at a time can be compared to cracks which develop one at a time, leaving the pattern of the force-displacement curve and complete pull-out unchanged.

4.2. *Extracting the pull-out load and stiffness data*

Fig. 7 shows the force-displacement data of the pull-out tests for the Honeycomb and Gyroid insert concepts. The data shows that the pull-out load of each specimen set varies within a few hundred Newton. This variation makes it more difficult to derive statements about which insert allows a higher load introduction. Valid statements about the potential of each insert concept require a statistical analysis, in which the average pull-out load of each set has been computed by adding all values of one

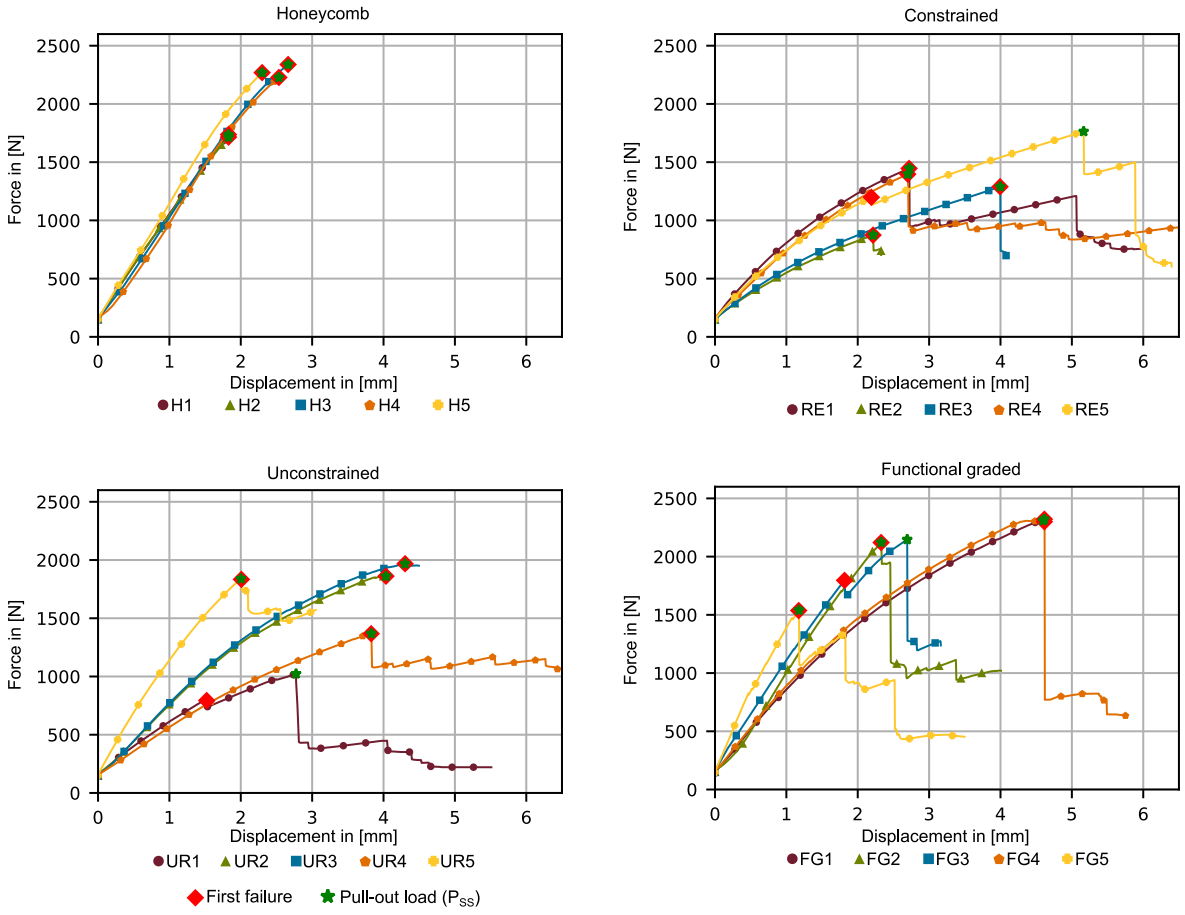

Fig. 7. Force displacement curves of the different specimens. Also included is the first failure and pull-out load.

set and normalizing it on the specimen size. Table A.9 summarises the results of such statistical analysis, whereas Fig. 9 visualises them. The right-hand side diagram of Fig. 9 shows the specific pull-out loads, which are normalised by the density of the specimens. The specific pull-out load removes the dependency on the relative density and helps to identify the potential of the functional grading.

Each column in Fig. 9 is accompanied by an error bar representing the data's variation by its standard deviation. For five specimens and assuming a Student's t-distribution, the standard deviation allows to estimate the 95 % confidence interval (CI). The 95 %-CI of the different concepts overlap significantly, discouraging direct conclusions. To address this issue, statistical tests were conducted using the Welch-Test method. It is a variation of the *t*-test, which considers each data set's variability and specimen quantity. The relations between the different specimen sets' absolute and specific pull-out loads can be obtained by executing multiple tests. For each test, it is necessary to provide a null hypothesis, which is assumed to be true and will then be tested. All specific hypotheses for the average pull-out load are derived from the column bar diagram in Fig. 9 and documented in Table 4. Each hypothesis is a single statement about two expectancy values μ of two specimen sets. The same hypothesis is used for the absolute and specific pull-out load. Results for both cases are provided in the form of the t- and p-value and the acceptance or denial of the null hypothesis.

The first two hypotheses, summarised in Table 4, compare Honeycombs to the G-UR and G-RE specimens. The results of the Welch tests indicate that the Honeycomb concepts possess an increased absolute pull-out load compared to the Gyroid concepts. However, using the specific pull-out load in the same hypothesis indicates the Gyroid concepts possess a superior or equal pull-out load. Both results are expected to be caused by the manufacturing error of the Honeycombs, where two out of six walls possess higher wall thicknesses. This additional mass increases the pull-out load slightly but not as much as evenly distributed material would. Therefore, the difference between the specific pull-out load of Honeycombs and Gyroids decreases enough to change the result of the Welch tests.

The statistical comparison of the Honeycomb and Gyroid insert concepts shows that similar specific pull-out loads can be achieved at similar insert and sandwich dimensions. Both are important because the failure of the insert is connected to the panel's failure. Therefore, the overall pull-out load depends on the potting diameter, height, relative density of the core and geometry of the face sheets. In this study, all parameters are kept the same as much as possible so that only the core type differs. Under these conditions and similar specific pull-out load values for both core types, it can be further concluded that the moment of area of the Honeycomb and Gyroid core must also be similar. A numerical investigation of the moment of area of the two cell types will be conducted in section 4.3 to gain additional insight.

By comparing the absolute and specific pull-out load of the graded TPMS concept with other concepts, this study assesses the potential of graded TPMS for improving insert efficiency. The results clearly indicate an improvement in the absolute and specific pull-out load due to the functional grading. Since the graded concept concentrates mass around the insert, where high loads are expected in the core structure, the specific pull-out load of the graded concept exceeds all other concepts. Since more material in the sandwich core increases the load-bearing capability, efficient material placement can only be determined with the density normalised relations. If the mass placement would not impact the specific pull-out load, no significant difference in the mean value could be observed. Both the column diagram in Fig. 9 and the corresponding Welch tests indicate that a significant difference can be

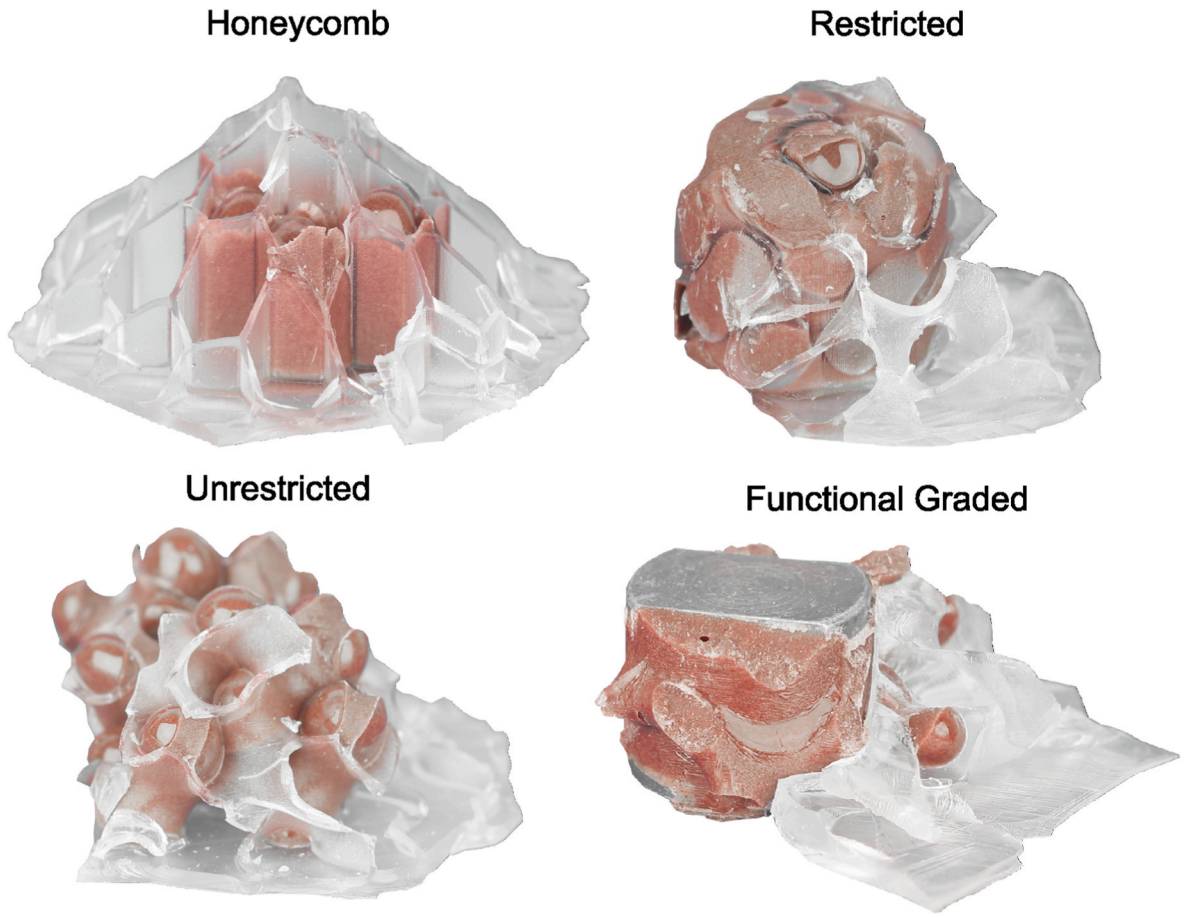

Fig. 8. Photographs of inserts which are completely pulled out of the Sandwich structure. Displayed are the specimens H3, G-RE4, G-UR4, G-FG2.

observed. In this case the certainty of the test results drop from 95 % for the absolute to 90 % for the specific pull-out load as the p-value indicates. The inadequate ratio between the diameter of the polymer branches and the wall thickness close to the insert is expected to contribute to this variability in the results. It is assumed that in the case of a more balanced relation, the confidence and also the specific pull-out load can be increased by the graded concept even further.

Next to their pull-out load, the stiffness that threaded inserts show in pull-out testing can be used to compare their mechanical potential. Fig. 7 allows an initial assessment of the stiffness of the inserts based on their force-displacement relationship. In every set, each curve shows a degressive trend, meaning that the stiffness continuously reduces with increasing displacement. Such a behaviour is known as visco-elastic behaviour and is a common characteristic of polymers. Comparing the Honeycomb and Gyroid force-displacement relationship, the authors observe a more rapid stiffness decrease in the Gyroid specimen. The difference is reasonable considering the local stress distribution, which is different in both structures.

The stiffnesses that the specimens of each Gyroid concept show are not randomly distributed but can be divided into subsets of specimens sharing the same stiffness properties. Especially the G-UR specimens show two specimen subsets sharing a similar stiffness. While geometry differences of the potting could, in theory, be accountable for the stiffness variations in the G-UR and G-FG concepts, the by-design non-existing differences in the G-RE concept suggest that the observed stiffness variations cannot be attributed to geometric differences in the potting, ruling out this factor as a source of variation. All specimens are manufactured from the same material, which suggests to justify ruling out the material as a source of variation as well. However, the variation in laser intensity during the printing process may cause a local change in material properties. The Formlabs Form 3 L has two areas that use their own laser. Honeycomb specimens reached across both areas, so each laser participated equally in curing all specimens. In the case of the Gyroid specimen, each was built in a different area and by a different laser. The polymerisation grade and stiffness would differ if the two lasers differ in intensity.

Comparing the different insert concepts requires one representative stiffness value for each concept. Due to the visco-elastic material behaviour, the stiffness differs at each point in the force-displacement diagram. It is assumed that visco-elasticity has little effect in regions of small deformations and forces. The maximum stiffness is chosen and computed by a moving average with a window of 100 values to obtain a single representative value. All stiffness properties, which were computed, are documented in Table A.10 and displayed in their absolute and density normalised form in Fig. 10. The error bars in the diagram show the 95 % confidence interval of the measured stiffness properties.

Analogous to the average pull-out load, the stiffness' standard deviation and confidence intervals of the different concepts overlap significantly. The Welch tests, also used to compare the pull-out load of the insert concepts, are now conducted to compare the stiffness of the insert concepts. All tested hypotheses are provided in Table 5 with their *t*- and *p-value*, as well as a statement, which indicates whether the hypothesis has been accepted or denied. The tests show that the stiffness properties of the Honeycomb insert concept exceed that of the Gyroid G-UR and G-RE concepts in terms of absolute stiffness but not in terms of specific stiffness. Therefore, it is concluded that the Honeycomb fastening points are not stiffer than the ones in the Gyroid cores. The higher absolute value is attributed to the manufacturing imperfections of the Honeycomb specimens, which lead to a higher relative density of the Honeycomb core compared to the Gyroid specimens.

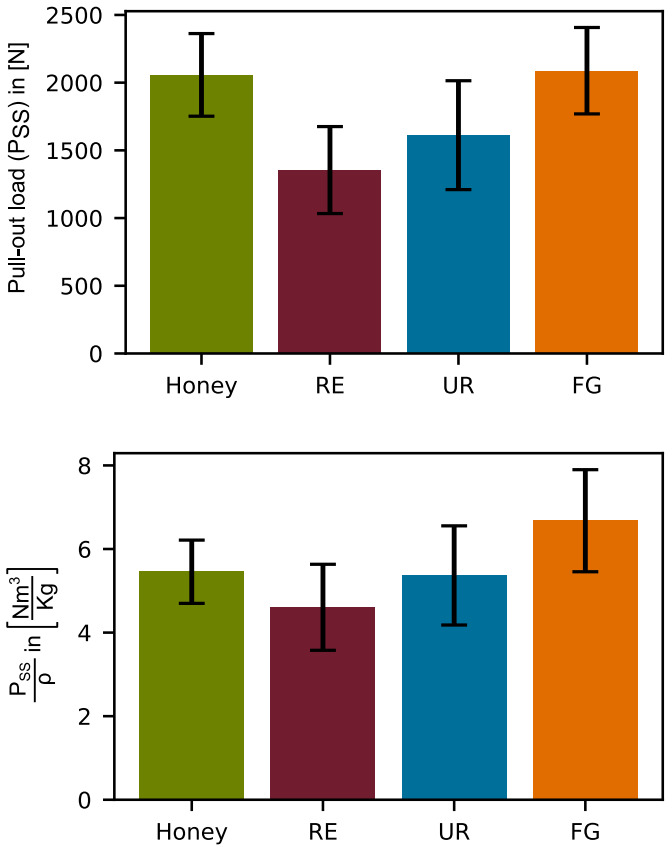

Fig. 9. Each set's average pull-out load is represented in column form. Error bars indicate standard deviation. The density values of Table A.9 have been used for the normalisation.

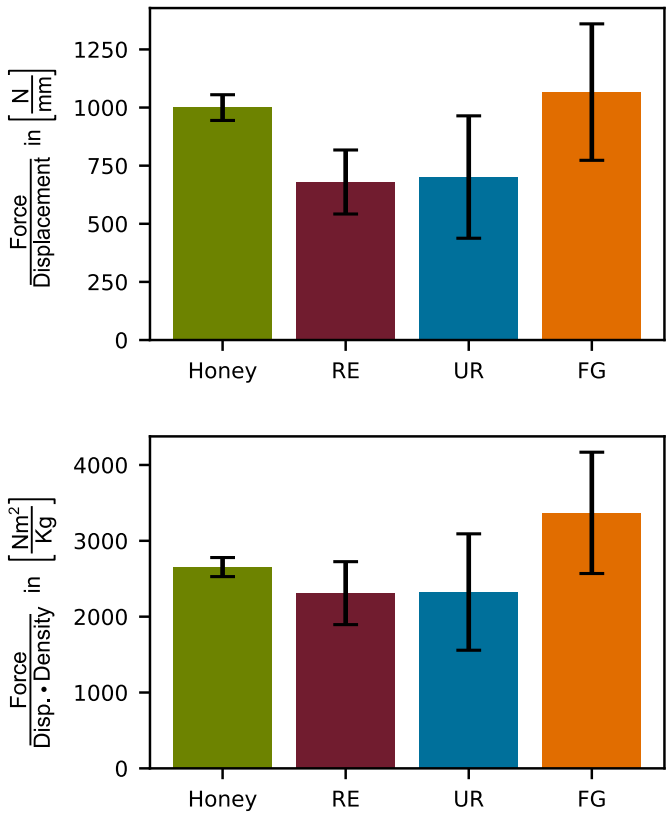

Fig. 10. The maximum Stiffness values are represented in column format with error bars indicating the standard deviation. The density values of Table A.6 are used for the normalisation.

Table 4
Welch-Test results about the average pull-out load.

Hyp 0	Hyp 1	Typ	t-value	p-value	Result
$\mu_{UR} < \mu_H$	$\mu_{UR} \geq \mu_H$	Force	−1.98	0.0434	True
		n. Force	−0.15	0.4464	False
$\mu_{RE} < \mu_H$	$\mu_{RE} \geq \mu_H$	Force	−3.55	0.0038	True
		n. Force	−1.49	0.0891	False
$\mu_{RE} < \mu_{UR}$	$\mu_{RE} \geq \mu_{UR}$	Force	−1.12	0.1485	False
		n. Force	−1.09	0.1550	False
$\mu_{UR} < \mu_{FG}$	$\mu_{UR} \geq \mu_{FG}$	Force	−2.08	0.0368	True
		n. Force	−1.72	0.0620	False

Decision criterion: Accept H0: $\mu_a < \mu_b$ if p-value $< p_{crit} = 0.05$ and t-value < 0.

Table 5
Welch-Test results about the average maximum stiffness.

Hyp 0	Hyp 1	Typ	t-value	p-value	Result
$\mu_{UR} < \mu_H$	$\mu_{UR} \geq \mu_H$	Stiffness	−2.49	0.0315	True
		n. Stiff.	−0.95	0.1976	False
$\mu_{RE} < \mu_H$	$\mu_{RE} \geq \mu_H$	Stiffness	−4.83	0.0021	True
		n. Stiff.	−1.78	0.0700	False
$\mu_{RE} < \mu_{UR}$	$\mu_{UR} \geq \mu_{RE}$	Stiffness	−0.17	0.4389	False
		n. Stiff.	−0.04	0.4857	False
$\mu_{UR} < \mu_{FG}$	$\mu_{UR} \geq \mu_G$	Stiffness	−2.08	0.0362	True
		n. Stiff.	−2.11	0.0342	True

Decision criterion: Accept H0: $\mu_a < \mu_b$ if p-value$< p_{crit} = 0.05$ and t-value< 0.

The functionally graded Gyroid insert concepts exhibit significantly higher stiffness than those without functional grading. The Welch tests on the absolute and specific stiffness underline the superior stiffness performance of the functionally graded inserts. The results are consistent with Fig. 10, where the G-FG insert concept shows the highest absolute and specific stiffness. The efficiency increase is caused by adding mass only at locations of high deflection. The deflection depends on the bending moment, divided by the moment of area and Young's modulus. While the modulus of both structures is identical, the moment of area depends on the cross-section geometry and density. In the functionally graded G-FG concept, the relative density is highest at the location of the highest bending moment, causing the biggest resistance against bending deflection and, therefore, the highest specific stiffness. Therefore, the mass used for the functional grading is efficiently distributed and creates a stiffer structure.

4.3. Computing the moment of area for both cell types

The force-displacement data from the pull-out experiments suggest that the Honeycomb and Gyroid Sandwich panels have remarkably similar average pull-out load and stiffness properties. Since the moment of area dictates the stress in the face sheets which were destroyed first, this leads to the conclusion that the moment of area of the different core structures must be similar. To support this conclusion and provide information for future research, the moment of area has been computed for a Honeycomb and Gyroid unit cell, depending on their relative density.

To calculate the moment of area of arbitrary unit cells, this study introduces a bitmap-based algorithm to numerically determine an averaged moment of sliced, three-dimensional geometries. The Python SDF library [26] is used to construct the geometry of Honeycomb and Gyroid unit cells as visualized in Fig. 11. For the Honeycomb cell a size of $l_{uc} = 6.66$ mm is used, while the Gyroid cell has dimensions of $l_{uc} = 10$

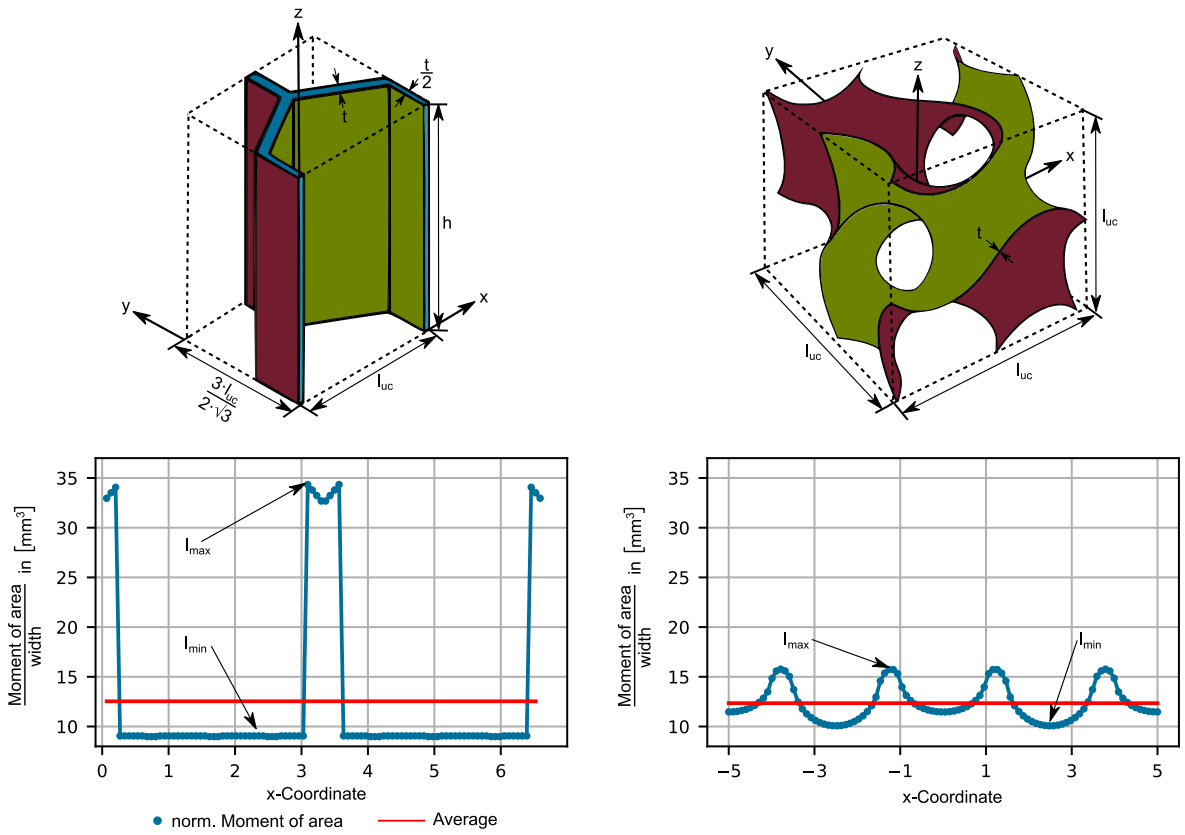

Fig. 11. Graphical illustration of the moment of area of a Honeycomb and Gyroid cell against bending around the y-axis. Both curves are related to a unit cell of 15% relative density. Above the curves, the corresponding cells are displayed with their unit cell boundaries.

mm. The general idea is to create slices of the unit cells and compute the moment of area for each slice. Each cell has been divided into 100 slices, which are distributed evenly along the x-axis. The moment of area around the x-axis is therefore computed depending on the x-position. The authors expect the honeycomb unit cell to have unequal moments of area in all three directions. The complete relationship is obtained if the process is repeated for multiple relative densities.

The graphs in the lower part of Fig. 11 show the local variation of the normalised moment of area within the Honeycomb and Gyroid unit cell. The displayed relationships originate from unit cells with a relative density of about 15 %. As mentioned before, the cell sizes are 10 mm for a Gyroid and 6.66 mm for a Honeycomb cell and therefore not identical. To be able to compare the two structures, the moment of area has been normalised on the width of the cell. The curve for the Honeycomb cell contains constant and short linear parts, while the Gyroid curve has an oscillating character. Both curves seem reasonable since Honeycombs are built out of flat walls and Gyroids out of sine and cosine functions. Their geometric character is, therefore, transmitted into the moment of area, indicating that the algorithm is working properly.

Comparing the moment of area of different unit cell geometries for the entire relative density range requires a representative value for each relative density. This study uses the average and the maximum to minimum ratio of the moment of area for such a comparison. The change in relative density is realised by modifying the wall thickness at a constant unit cell length. In this case, the moment of area has been normalised on the moment of area of a solid block I_{cube} with the same dimensions $l_{uc} = 10$ mm for the Gyroid and $l_{uc} = 6.66$ mm for the Honeycomb cell.

The relationship between the average moment of area and the relative density of Gyroid and Honeycomb unit cells is displayed in the upper diagram of Fig. 12. The moments of area for the rotation around the y- and x-axis are both included in the graph. Since both moments are identical, the graphs overlap, and only one graph is visible in the diagrams. The Gyroid and Honeycomb cell both follow a linear trend and align almost perfectly up to a relative density of 60 %. In higher regions, the curves split, and while the Honeycomb curve continues to be linear, the Gyroid shows a minor peak. The authors expect the non-linear behaviour of the Gyroid sheet networks at high relative densities to be connected to an uneven thickness of the channels inside the structure, forming voids when further increasing the relative density. The voids are then within the unit cell, while the outer regions of the unit cell are already solid, thus increasing the area moment disproportionately high.

According to the data provided by the calculations, the initial hypothesis that both moments of area must be equal can be accepted for the global moment of area within one unit cell. At the same time, significant local variations occur, so it is questionable whether a global model of the moment of area is sufficient to describe the mechanical behaviour of the unit cells. A first impression which supports this argument provides the lower diagram of Fig. 12. The diagram shows the ratio between the maximum and minimum moment of area as marked in Fig. 11 for both unit cells. The ratio is displayed depending on the relative density and for a rotation around the y- and x-axis. In this case, both axes are still the same for a Gyroid unit cell but differ for a Honeycomb one. The curves for a Honeycomb cell show a much larger ratio than the Gyroid cell, indicating that much higher stress concentrations should occur in a Honeycomb cell while bending around the given axis. Whether this hypothesis is valid remains the subject of further research. More specific beam bending tests, which are specialized in investigating the relation between the local and global moment of area, are needed to provide the corresponding insight.

5. Discussion and conclusion

The authors of this study developed three different concepts for

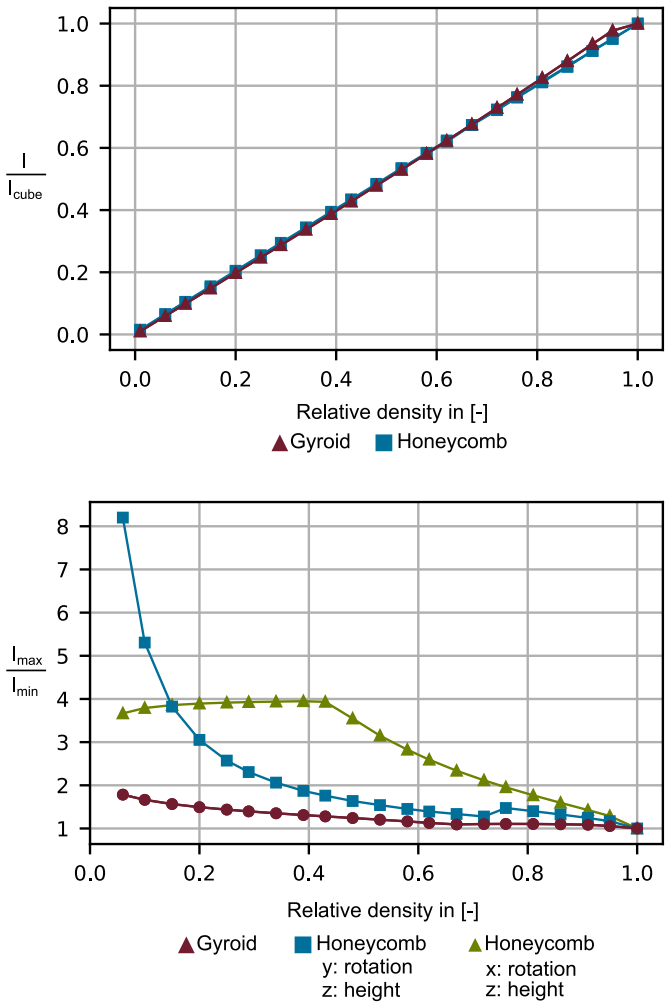

Fig. 12. The normalised moment of area over the relative density for a Gyroid and Honeycomb unit cell (upper). The ratio of maximum and minimum moment of area (lower).

threaded inserts in TPMS sandwich structures and compared their performance to industrially available concepts for Honeycomb sandwich structures. The insert performance was assessed by conducting and evaluating pull-out experiments on the additive-manufactured sandwich specimens with integrated threaded inserts. The results show that the TPMS insert concepts tested by example on the Gyroid structure have a similar stiffness and pull-out load as the Honeycomb inserts. Functionally grading the Gyroid structure in the proximity of the threaded insert showed a significant potential for performance improvements.

The pull-out experiments conducted in this study on threaded inserts showed no significant difference in the average pull-out load and stiffness between the Gyroid and Honeycomb concepts at the same relative densities. Therefore, applying the design rules defined for Honeycomb sandwich structures by the insert design handbook [24] to Gyroid concepts looks promising. A more detailed assessment of the applicability of the design rules requires additional research on TPMS inserts with larger variations in the ratio of insert and sandwich size.

All specimens tested in this study initially failed in the face sheet. Therefore, this study offers no insights into the behaviour of TPMS inserts in scenarios where the initial failure is in the sandwich core. However, the macroscopic form fit between the potting and the Gyroid core suggests that the Gyroid inserts achieve a higher pull-out load compared to Honeycomb inserts. This hypothesis can be tested by increasing the wall thickness of the face sheets to increase their load-bearing proportion or by joining the TPMS core structure with face sheets of higher strength and stiffness, such as carbon fibre-reinforced plastics. For testing larger variations of insert and sandwich core sizes, the authors suggest employing a FEM model for such variations and validating it with a limited number of experiments.

In all pull-out experiments, the Gyroid core structure showed a crack-stopping behaviour, resulting in residual load-bearing capability after initial failure. Such a behaviour is extremely beneficial in any application with safety concerns. Sandwich structures with a Gyroid core mounted to other structures would not detach after initial failure. While the initial failure of the panel at the fastening point results in large deformation and can, therefore, be detected, in the best-case scenario, the sandwich structure can still maintain its original functionality.

Functionally graded Gyroid sandwich structures showed the benefits of a relative density gradient in the proximity of the inserts during pull-out testing. Adding a relative density gradient increases the load-per-weight ratio, which can be introduced into the sandwich structure. Therefore, functional grading can be highly recommended for light-weight structures where significant mass savings and proportionally high load transfers are required. The results of this study highlight the importance of the ratio between the core structure's wall thickness and the potting branches' diameter when applying functional grading of the relative density in TPMS sheet networks. An optimum ratio is archived when the geometry and material strength of the walls and branches are in balance. In this study, the balance was shifted in favour of the core structure walls, resulting in a reduced pull-out load of the insert. However, the load-bearing capability of functionally graded structures is expected to be further improved by carefully considering the strength ratio between the potting and core structure.

The pull-out experiments conducted in this study on Gyroid and Honeycomb sandwich panel specimens with equal relative densities of the core structure demonstrated similar pull-out loads and bending stiffnesses. To investigate the reason for this result, a numerical study compared the average moment of area of the Gyroid and Honeycomb structures as a function of relative density. The study showed that the two structures have equal moments of area for equal relative densities, which explains the observed similar pull-out load and stiffness of the sandwich panel specimens.

The studies of Fashanu et al. [11] and Alshaer et al. [12] investigated the three-point bending behaviour of TPMS sandwich panels as mentioned in the introduction 1. The loading state of the three-point bending test is similar to the pull-out test's. Results from this study can be related to results obtained by the two investigations, thus providing further insight into the contradicting results of both studies regarding the stiffness of Gyroid and Honeycomb cores. The results of this study show similar stiffnesses for a Honeycomb and Gyroid core with similar relative densities, backed by the computations of the moment of area, which is also equal. The data provided by Fashanu et al. is in line with these results, and an identical stiffness was observed for both core structures. This is not true for the study of Alshaer et al. [12], where the authors claim that the stiffness of a Gyroid sandwich is about twice as high compared to a honeycomb sandwich. Based on the information provided by the authors, the exact reason for this deviation cannot be determined. However, one hypothesis could be a significant difference in the adhesive layer height, which connects the face sheets to the core. Differences in layer height at this place greatly impact the moment of area, directly affecting the stiffness. Although two out of three studies report the same results, an additional study to validate the concept of the mean moment of area is suggested here.

In summary, this study investigates the performance of threaded inserts in additive-manufactured TPMS sandwich structures compared to Honeycombs manufactured by the same process. The results showed that the Gyroid TPMS insert concepts had a similar stiffness and pull-out load compared to the Honeycomb inserts. Moreover, the Gyroid core structure showed a crack-stopping behaviour, resulting in a residual load-bearing capability after the first failure, making it highly beneficial for applications with safety concerns. The study also demonstrated the

potential of functional grading in the proximity of the threaded insert for performance improvements. However, the study had limitations, such as face sheet failure, so further investigations are necessary, such as varying the ratio of sandwich and insert size by utilizing a FEM model with experimental validation. The functional grading can also be improved by optimizing the ratio of walls and potting branches. Overall, the study suggests that sandwich structures with Gyroid infill are a promising technology for local load introduction and justifies further research in this area.

CRediT authorship contribution statement

David Lohuis: Conceptualization, Data curation, Formal analysis, Investigation, Methodology, Software, Validation, Visualization, Writing – original draft, Writing – review & editing. **Hendrik Traub:** Conceptualization, Funding acquisition, Investigation, Methodology, Project administration, Software, Supervision, Validation, Visualization, Writing – original draft, Writing – review & editing. **Christian Hühne:** Funding acquisition, Project administration, Resources, Supervision, Writing – review & editing.

Declaration of generative AI and AI-assisted technologies in the writing process

During the preparation of this work, the authors used ChatGPT to suggest improvements in language and readability. After using this tool, the authors reviewed and edited the content as needed and take full responsibility for the content of the publication.

Declaration of competing interest

The authors declare that they have no known competing financial interests or personal relationships that could have appeared to influence the work reported in this paper.

Data availability

Data will be made available on request.

Acknowledgments

This research was funded by the Deutsche Forschungsgemeinschaft (DFG, German Research Foundation) under Germany's Excellence Strategy – EXC 2163/1-Sustainable and Energy Efficient Aviation – Project-ID 390881007 and by the German Federal Ministry for Economic Affairs and Climate Action (BMWK) under project number 20A2103D (MuStHaF).

Appendix A. Statistical analysis

Table A.6
Absolute density ρ $[\frac{Kg}{m^3}]$

Specimen	H	RE	UR	FG
1	359.18	300.19	284.53	301.14
2	358.17	285.2	301.62	318.37
3	364.40	284.76	302.63	319.87
4	358.04	299.72	287.29	302.99
5	367.14	296.405	316.89	329.57
Average	361.38	293.25	298.59	314.39
Variance	17.14	59.19	34.29	145.46
Std.-dev.	4.14	7.69	5.86	12.06
rel.Std.	1.15%	2.62%	2.00%	3.83%

Table A.7
Total mass ***m*** in [g]

Specimen	H	RE	UR	FG
1	119.7	96.7	91.9	97.7
2	119.5	91.5	97.4	102.9
3	122.5	91.3	97.9	103.5
4	121.0	95.9	93.6	98.3
5	123.5	95.2	101.6	105.5
Average	121.24	94.12	96.48	101.58
Variance	3.04	6.45	14.59	9.32
Std.-dev.	1.74	2.54	3.82	3.05
rel.Std.	1.4%	2.7%	4.0%	3.0%

Table A.8
Potting mass ***m*** in [g]

Specimen	H	RE	UR	FG
1	2.37	2.0	1.1	0.2
2	2.47	2.8	2.2	0.8
3	2.57	2.5	2.3	1.3

(*continued on next page*)

Table A.8 (*continued*)

Specimen	H	RE	UR	FG
4	2.96	2.5	2.5	0.7
5	3.08	2.5	2.6	0.7
Average	2.69	2.46	2.40	0.74
Variance	0.098	0.083	0.36	0.15
Std.-dev.	0.31	0.29	0.62	0.39
rel.Std.	11.52%	11.79%	25.83%	52.70%

Table A.9
Average pull-out load P_{SS} in [N]

Specimen	H	RE	UR	FG
1	1736.72	1447.29	1023.15	2321.17
2	1715.27	874.06	1861.22	2122.82
3	2338.55	1289.75	1968.22	2146.9
4	2227.37	1397.56	1368.53	2309.42
5	2268.83	1763.47	1839.42	1540.9
Aver.	2057.35	1354.43	1612.11	2088.24
Var.	74505.27	82547.15	129349.01	81478.96
St.dev.	272.96	287.31	359.65	285.45
rel.St.	13.27%	21.21%	22.31%	13.67%

Table A.10
Average maximum stiffness $\boldsymbol{D}$ in $[\frac{N}{mm}]$

Specimen	H	RE	UR	FG
1	953.95	866.42	594.11	806.56
2	958.56	532.83	652.48	1035.46
3	967.72	555.58	672.35	1192.65
4	1047.16	707.63	442.80	797.70
5	1071.66	736.26	1143.64	1500.00
Av.	999.81	679.74	701.08	1066.474
Var.	3059.73	18955.01	69299.47	86155.45
St.dev.	55.31	137.68	263.25	293.52
rel.St.	5.53%	20.25%	37.55%	27.52%

Appendix B. Relative density formula

$$RD_H = \frac{\rho_{cell}}{\rho_{solid}} = \frac{V_{cell}}{V_{solid}} = \frac{A_{cell}}{A_{solid}} \tag{B.1}$$

$$A_{cell} = A_1 + A_2 \tag{B.2}$$

$$A_1 = \frac{t}{2}\left(\frac{\sqrt{3}}{6}(l_{uc} - t)\right) = \frac{\sqrt{3}}{12}(l_{uc}t^2 - t) \tag{B.3}$$

$$A_2 = \frac{1}{2} * \frac{\sqrt{3}}{6} t * \frac{1}{2} t = \frac{\sqrt{3}}{24} l_{uc}^2 \tag{B.4}$$

$$A_{ges} = \frac{1}{2} * \frac{l_{uc}}{2} * \frac{\sqrt{3}}{6} l_{uc} = \frac{\sqrt{3}}{24} l_{uc}^2 t \tag{B.5}$$

$$\rho_{rel} = 2\frac{t}{l_{uc}} - \frac{t^2}{l_{uc}^2} \tag{B.6}$$

References

[1] L.J. Gibson, M.F. Ashby, Cellular solids: structure and properties, in: Cambridge Solid State Science Series, second ed., Cambridge Univ. Press, Cambridge, 1997.

[2] V. Birman, G.A. Kardomateas, Review of current trends in research and applications of sandwich structures, Compos. B Eng. 142 (2018) 221–240, https://doi.org/10.1016/j.compositesb.2018.01.027.

[3] A. Nazir, K.M. Abate, A. Kumar, J.-Y. Jeng, A state-of-the-art review on types, design, optimization, and additive manufacturing of cellular structures, Int. J. Adv. Des. Manuf. Technol. 104 (9–12) (2019) 3489–3510, https://doi.org/10.1007/s00170-019-04085-3.

[4] H. Traub, M. Sprengholz, D. Teufel, C. Hühne, Structural-mechanical characterisation of triply periodic minimal surface sheet networks: simulation and experiment, in: AIAA SCITECH 2023 Forum, American Institute of Aeronautics and Astronautics, Reston, Virginia, 2023, pp. 1–28, https://doi.org/10.2514/6.2023-2076.
[5] H. Traub, J. Wolff, S. Jose, L. Lobitz, M. Schollerer, C. Hühne, Concept and design of extended hybrid laminar flow control suction panels, Sci. Rep. (2021), https://doi.org/10.21203/rs.3.rs-924184/v1.
[6] S. Heimbs, M. Pein, Failure behaviour of honeycomb sandwich corner joints and inserts, Compos. Struct. 89 (4) (2009) 575–588, https://doi.org/10.1016/j.compstruct.2018.05.105.
[7] G. Qi, L. Ma, Experimental investigation of composite pyramidal truss core sandwich panels with lightweight inserts, Compos. Struct. 187 (December) (2018) 336–343, https://doi.org/10.1016/j.compstruct.2017.12.071.
[8] G. Qi, Y.-L. Chen, P. Rauschen, K.-U. Schröder, L. Ma, Characteristics of an improved boundary insert for sandwich panels with lattice truss cores, Aero. Sci. Technol. 107 (2020) 106278, https://doi.org/10.1016/j.ast.2020.106278.
[9] G. Qi, Y.-L. Chen, P. Richert, L. Ma, K.-U. Schröder, A hybrid joining insert for sandwich panels with pyramidal lattice truss cores, Compos. Struct. 241 (January) (2020) 112123, https://doi.org/10.1016/j.compstruct.2020.112123.
[10] O. Al-Ketan, R.K.A. Al-Rub, Multifunctional mechanical metamaterials based on triply periodic minimal surface lattices, Adv. Eng. Mater. 21 (10) (2019) 1900524, https://doi.org/10.1002/adem.201900524.
[11] O. Fashanu, M. Rangapuram, A. Abutunis, J. Newkirk, K. Chandrashekhara, H. Misak, D. Klenosky, Mechanical performance of sandwich composites with additively manufactured triply periodic minimal surface cellular structured core, J. Sandw. Struct. Mater. (2021), https://doi.org/10.1177/10996362211037012, 109963622110370.
[12] A.W. Alshaer, D.J. Harland, An investigation of the strength and stiffness of weight-saving sandwich beams with CFRP face sheets and seven 3D printed cores, Compos. Struct. 257 (November 2020) (2021) 113391, https://doi.org/10.1016/j.compstruct.2020.113391.
[13] J. Schwenke, D. Krause, Optimization of load introduction points in sandwich structures with additively manufactured cores, Des. Sci. 6 (2020) e13, https://doi.org/10.1017/dsj.2020.10.
[14] F. Schulte, J. Würtenberger, K.-E. Steffan, E. Kirchner, TRIZ als Schlüssel zu den Potentialen additiver Fertigungsverfahren, in: Konstr. für die Addit. Fert. 2018, Springer Berlin Heidelberg, Berlin, Heidelberg, 2020, pp. 55–75, https://doi.org/10.1007/978-3-662-59058-4_4.
[15] Formlabs, Form 3L: The First Affordable Large SLA 3D Printer, 2022 27.09. ULR https://formlabs.com/3d-printers/form-3l/.
[16] J.P. Cushman, R.J. Murphy, Geometric Considerations in the Design of Honeycomb Sandwich Fasteners, 1966, https://doi.org/10.2514/3.28729.
[17] G. Bianchi, G.S. Aglietti, G. Richardson, Optimization of bolted joints connecting honeycomb panels, in: Proc. The10th Eur. Conf. Spacecr. Struct. Mater. Mech. Test., 2007, pp. 10–13. URL, http://eprints.soton.ac.uk/65075/.
[18] N. Raghu, M. Battley, T. Southward, Strength variability of inserts in sandwich panels, J. Sandw. Struct. Mater. 11 (6) (2009) 501–517, https://doi.org/10.1177/1099636209104524.
[19] GmbH 3M Deutschland, Technical Data Sheet - 3M - Scotch Weld 9300 BA/FST. Access Date: 3.March 2022 Access Time: 01:45 p.M, 2011. URL, https://multimedia.3m.com/mws/media/749734O/3mtm-scotch-weldtm-9300-b-a-fst-two-part-structural-adhesive.pdf.
[20] O.T. Thomsen, Analysis of the Sandwich Panels with "Through-The-Thickness" Inserts Using a Higher-Order Sandwich Plate Theory, ESA, Noordwijk, Netherlands, 1994.
[21] E. Bozhevolnaya, A. Lyckegaard, O. Thomsen, V. Skvortsov, Local effects in the vicinity of inserts in sandwich panels, Composites, Part B 35 (6–8) (2004) 619–627, https://doi.org/10.1016/j.compositesb.2003.09.003.
[22] J. Wolff, M. Brysch, C. Hühne, Validity check of an analytical dimensioning approach for potted insert load introductions in honeycomb sandwich panels, Compos. Struct. 202 (2018) 1195–1215, https://doi.org/10.1016/j.compstruct.2018.05.105.
[23] W.C. Inc, NAS1836-08-11 Data Sheet. Access Date: 20.January 2023, Access Time 08:40 a.M, 2023. URL, https://www.wittenco.com/?page_id=47.
[24] I.D.H. ECSS, Insert Design Handbook, ESA Requirements and Standards Division, 2011.
[25] Autodesk, Fusion 360. Access Date: 3.March 2022, Access Time: 01:45 p.M, 2022. URL, https://www.autodesk.de/products/fusion-360/personal.
[26] sdf Bibliothek Fogleman, Access Date: 3.March 2022, Access Time: 01:45 p.M, 2021. URL, https://github.com/fogleman/sdf.
[27] FormLabs, Standard Materials - Data Sheet. Access Date: 3.March 2022, Access Time: 01:45 p.M, 2017. URL, https://formlabs-media.formlabs.com/datasheets/Standard-DataSheet.pdf.
[28] FormLabs, Form Wash, Access Date: 9.January 2023, Access Time: 03:03 p.m, 2023. URL, https://formlabs.com/post-processing/wash-cure/.
[29] FormLabs, Form Cure time and temperature settings, Access Date: 3.March 2022, Access Time: 01:45 p.m, 2021. URL https://support.formlabs.com/s/article/Form-Cure-Time-and-Temperature-Settings?language=en{_}US.
[30] Zwick ZwickRoell, Roell manufacturer, Access Date: 17.March 2023, Access Time: 03:19 p.m, 2023. URL, https://www.zwickroell.com/de/.
[31] DIN Deutsches Institut für Normung e. V, Normalklimate für die Probenvorbereitung und Prüfung, 2011. ISO 139:2011-10).
[32] G. Bianchi, G.S. Aglietti, G. Richardson, Static performance of hot bonded and cold bonded inserts in honeycomb panels, J. Sandw. Struct. Mater. 13 (1) (2011) 59–82, https://doi.org/10.1177/1099636209359840.